Computational Materials Science 107 (2015) 15–23

Contents lists available at ScienceDirect

Computational Materials Science

journal homepage: www.elsevier.com/locate/commatsci

First-principles study of Cd impurities localized at and near the (001) α-Al_2O_3 surface

Germán N. Darriba [a,*], Ricardo Faccio [b,c], Mario Rentería [a]

[a] Departamento de Física, Instituto de Física La Plata (IFLP, CONICET La Plata), Facultad de Ciencias Exactas, Universidad Nacional de La Plata, CC 67, 1900 La Plata, Argentina
[b] Crystallography, Solid State and Materials Laboratory (Cryssmat-Lab), DETEMA, Facultad de Química, Universidad de la República, Gral. Flores 2124, P.O. Box 1157, Montevideo, Uruguay
[c] Centro NanoMat, Polo Tecnológico de Pando, Facultad de Química, Universidad de la República, Cno. Aparicio Saravia s/n, 91000 Pando, Canelones, Uruguay

ARTICLE INFO

Article history:
Received 25 February 2015
Received in revised form 7 April 2015
Accepted 12 April 2015
Available online 26 May 2015

Keywords:
Impurity
Al_2O_3
Surfaces
DFT
EFG
Magnetic moment

ABSTRACT

A combination of two first-principles electronic structure calculation methods in the framework of density-functional theory was applied to investigate the (001) α-Al_2O_3 surface reconstruction and its structural, electronic, magnetic, and hyperfine properties when doped with Cd impurities at different depths from the surface. The SIESTA approach was used to obtain the equilibrium positions of all atoms and the Full-Potential Augmented Plane Wave plus local orbital (FP-APW+lo) method was employed in order to obtain the electronic structure at these equilibrium positions and all the other physical properties. For the most stable (001) α-Al_2O_3 surface, we have demonstrated that the inclusion of the Cd atom at substitutional Al sites at and near the surface produces a ground state magnetic behavior. The largest principal component V_{33} of the electric-field-gradient (EFG) tensor at the Cd atom localized just above the α-Al_2O_3 terrace showed the same [001] orientation and a dominating *p*-character as Cd does when it is localized at bulk α-Al_2O_3, but exhibits an anomalous V_{33} magnitude four times larger than its value in bulk. Just below the surface, the non symmetric structural relaxation around the Cd impurity is responsible for the strong change in the asymmetry, magnitude, and orientation of the EFG tensor. The changes in the hyperfine properties have been correlated with the modifications observed on the electronic charge density at the different Cd sites and on the *p*-states of the Cd-projected partial density of states. Accordingly, the significant differences on the hyperfine parameters showed for different depths suggest that ^{111}Cd probe-atoms used in Perturbed γ–γ Angular Correlation experiments could be used for evaluating geometrical and electronic distortions, particularly for positions quite close to the reconstructed surface, as well as contributing to studies of growth, adsorption, and diffusion of atoms in oxide surfaces and interfaces.

1. Introduction

The behavior of structural and electromagnetic properties as long as one approaches surfaces and interfaces is fundamental to get insight of the interatomic interactions present at these particular boundary conditions. The surface of α-Al_2O_3, and in particular its (001) surface, is a major interface because of its extensive use as substrates in microelectronics, spintronics [1,2], ultrathin technology [3,4] and, more recently, as substrate in superconducting qubit devices [5]. Related with the use of Al_2O_3 substrates in qubit devices for quantum computation applications, recent important investigations were driven to unravel the origin of the magnetic noise present in real samples, in order to passivate it [5]. In particular, the capability to passivate the magnetic noise in qubits systems based on (001) α-Al_2O_3 surfaces doped with metallic impurities at different depths should be investigated from first-principles. Therefore, the surface reconstruction and the understanding of the behavior of the alumina surface properties, in pure and as well as in doped systems, are relevant in both basic and applied physics.

One way to obtain physical information at the atomic scale in solids (among other systems) is to study hyperfine properties of suitable probe-atoms in the material under consideration. The magnetic hyperfine interactions at surfaces are important to understand the exchange interactions, whereas the quadrupole-electric hyperfine interactions are very sensitive to local electronic and structural modifications of the probe-atom neighborhood. Particularly, the electric-field-gradient tensor

* Corresponding author. Tel.: +54 221 4246062; fax: +54 221 4252006.
E-mail address: darriba@fisica.unlp.edu.ar (G.N. Darriba).

http://dx.doi.org/10.1016/j.commatsci.2015.04.008
0927-0256/

(EFG) at a given atom is a physical quantity strongly dependant on subtle variations of the electronic charge density anisotropy around the atomic nucleus (since the EFG depends on the distance from the source charges as r^{-3}). In effect, their components $V_{ij}(\vec{r}) = \frac{\partial^2 V(\vec{r})}{\partial x_i \partial x_j}$ are defined as the second derivate, with respect to the spatial coordinates, of the Coulomb potential $V(\vec{r})$ originated on the electric charges neighboring the nucleus. Since the EFG tensor is traceless in its principal axes system, it can be completely defined by only two quantities: V_{33} (its largest principal component, using the standard convention $|V_{33}| \geqslant |V_{22}| \geqslant |V_{11}|$) and the asymmetry parameter $\eta = (V_{11} - V_{22})/V_{33}$. In single crystalline samples the direction of the EFG tensor, defined as the orientation of the principal axes system with respect to the crystalline axes, can also be measured.

Experimentally, many hyperfine techniques [6,7] have been widely applied to nuclear condensed-matter physics in order to investigate at the atomic level, electronic, magnetic, and structural properties in both pure and doped systems, mainly in bulk [8]. Particularly, the subnanoscopic environment characterization of native or impurity atoms in solids can be obtained employing the Time-Differential Perturbed γ–γ Angular Correlations (TDPAC) spectroscopy [9–12], through the precise determination of the EFG tensor that it provides at diluted (ppm) suitable radioactive probe-atoms.

In the case of surfaces, Körner et al. [13] and Klas et al. [14–16] were the first to perform a detailed experimental TDPAC study of the EFG tensor at ^{111}Cd atoms located at the surface of metallic indium and copper, respectively, showing the potential of this technique to study surfaces through the characterization of the EFG tensor.

Nowadays, the EFG can provide valuable information about the studied system (structural deformations, localization and charge state of defect centers and impurities, character of impurity levels, etc.) confronting its experimental determination with very accurate EFG theoretical predictions [10,17–19], using all-electron (AE) *ab initio* electronic structure calculations in the framework of the density functional theory (DFT) [20,21].

As previous steps to the present work, we studied the structural, electronic, and hyperfine properties of isolated Cd atoms in bulk α-Al_2O_3 [18], and the local environment of reconstructed pure (001) α-Al_2O_3 surface [22]. Here, we present a detailed theoretical *ab initio* study for determining structural, electronic, magnetic, and hyperfine properties of isolated Cd impurities located at and near the (001) α-Al_2O_3 surface (at substitutional Al cationic sites), i.e., as a function of the Cd's depth with respect to this surface.

In one of the previous works we successfully employed two *ab initio* methods with different basis set (the Full-Potential Augmented Plane Wave plus local orbital (FP-APW+lo) method and a linear combination of numerical localized atomic-orbitals basis set, implemented in WIEN2k and SIESTA packages, respectively) for the understanding of the reconstruction of pure α-Al_2O_3 (001) surface [22]. In order to determine the electronic, magnetic, and hyperfine properties in the doped surfaces, we calculated the EFG using the FP-APW+lo method at the equilibrium atomic positions predicted by SIESTA since, as we showed in Ref. [22] for the pure surface, this method predicts final equilibrium structures with comparative lower energy than those predicted by the FP-APW+lo method.

Now, understanding the surface reconstruction and obtaining relevant electronic properties in the presence of Cd impurities, allow us to demonstrate the importance of this extremely sensitive local probe. Particularly, for evaluating electromagnetic and structural properties in the proximity of the Al_2O_3 surface.

2. Methodology

Following an analogous procedure for the study of the pure (001) α-Al_2O_3 surface [22], we started with the bulk α-Al_2O_3 unit cell in its hexagonal representation according to the R-3 c H space group using the following cell and internal parameters: a = 4.75999(3) Å and c = 12.99481(7) Å [23], u = 0.35219(1) and v = 0.30633(5) [23]. According to this, each aluminum atom presents six nearest oxygen neighbors (ONN), three of them located at 1.854 Å (O1) and the rest located at 1.972 Å (O2).

The (001) surface was modeled using the slab approximation, utilizing a standard unit cell and introducing vacuum along the [001] direction, see Fig. 1(a). A vacuum region of 14 Å probed to be sufficient in order to avoid interaction between adjacent images. The selected surface termination used as a starting point of all our calculations corresponds to the most stable optimized pure surface as determined in our previous work [22], which is in agreement with X-ray diffraction [24] and ion-scattering experiments [25,26]. In order to simulate an isolated impurity, a Cd atom replaces one of the Al atoms localized at the lattice sites shown in Fig. 1(b)–(g), obtaining a cationic impurity dilution of 1:12. In Ref. [18] we showed that this dilution is sufficient to simulate a Cd isolated impurity in bulk α-Al_2O_3. Thus, this dilution warrants the absence of undesired Cd–Cd interactions, in bulk as well as in the slab geometry, in order to be closer to the conditions of diluted probe atoms used in hyperfine experimental techniques. The Cd atom was located at the different Al cation sites shown in Fig. 1, varying the Cd depth from the surface. From here on we establish the following notation for the Cd-doped systems in the (001) α-Al_2O_3 surface: Al_2O_3:Cd_1 (Fig. 1(b)), when the Cd atom replaces the topmost Al atom, whereas Al_2O_3:Cd_i (i = 2–6), when the Cd atom replaces the corresponding Al atoms as we move away from the surface into the bulk (Fig. 1(c)–(g)).

Two different first-principles DFT implementations were selected in order to get the full geometrical reconstructions for the studied systems. The WIEN2k code [27] implements the FP-APW+lo method [28,29]. In this case the wave functions are expanded in spherical harmonics into non-overlapping spheres, and plane waves in the interstitial region. The spheres are delimited by the so-called muffin-tin radii (R_{MT}), and we selected for Al, O, and Cd the following values: 0.87, 0.85, and 1.10 Å, respectively. We used 32 k-points for the sampling of the irreducible wedge of the Brillouin Zone, using the tetrahedron method. The size of the basis is controlled by the $R_{MT}K_{\max}$ value, set to 7.0 in our case. The V_{ii} elements of the EFG tensor were obtained for each atom in the final optimized geometries. These elements were obtained from the V_{2M} components of the lattice harmonic expansion of the self-consistent potential [30]. The exchange and correlation (Exc) effects were treated using both the local-density approximation (LDA) [31] and the generalized gradient approximation (GGA). In particular for GGA we use the Perdew–Burke–Ernz erhof (PBE) parametrization [32]. The results obtained from both potentials probed to follow similar trends, for that reason we decided to present here just the results from GGA-PBE Exc-potential.

The SIESTA code [33–35] uses a linear combination of numerical localized atomic orbitals for describing the valence electrons, and norm-conserving non-local pseudopotentials for the description of the atomic core. The pseudopotentials were obtained following the Trouiller and Martins scheme [36]. We used a split-valence with double-ζ basis set, including polarization orbitals in all the atoms. The real-space extension of the numerical orbitals was determined from an energy confinement of 50 meV. We selected PBE-GGA for the description of the Exc-potential [32]. The charge density and wavefunctions is projected in a real-space grid, as

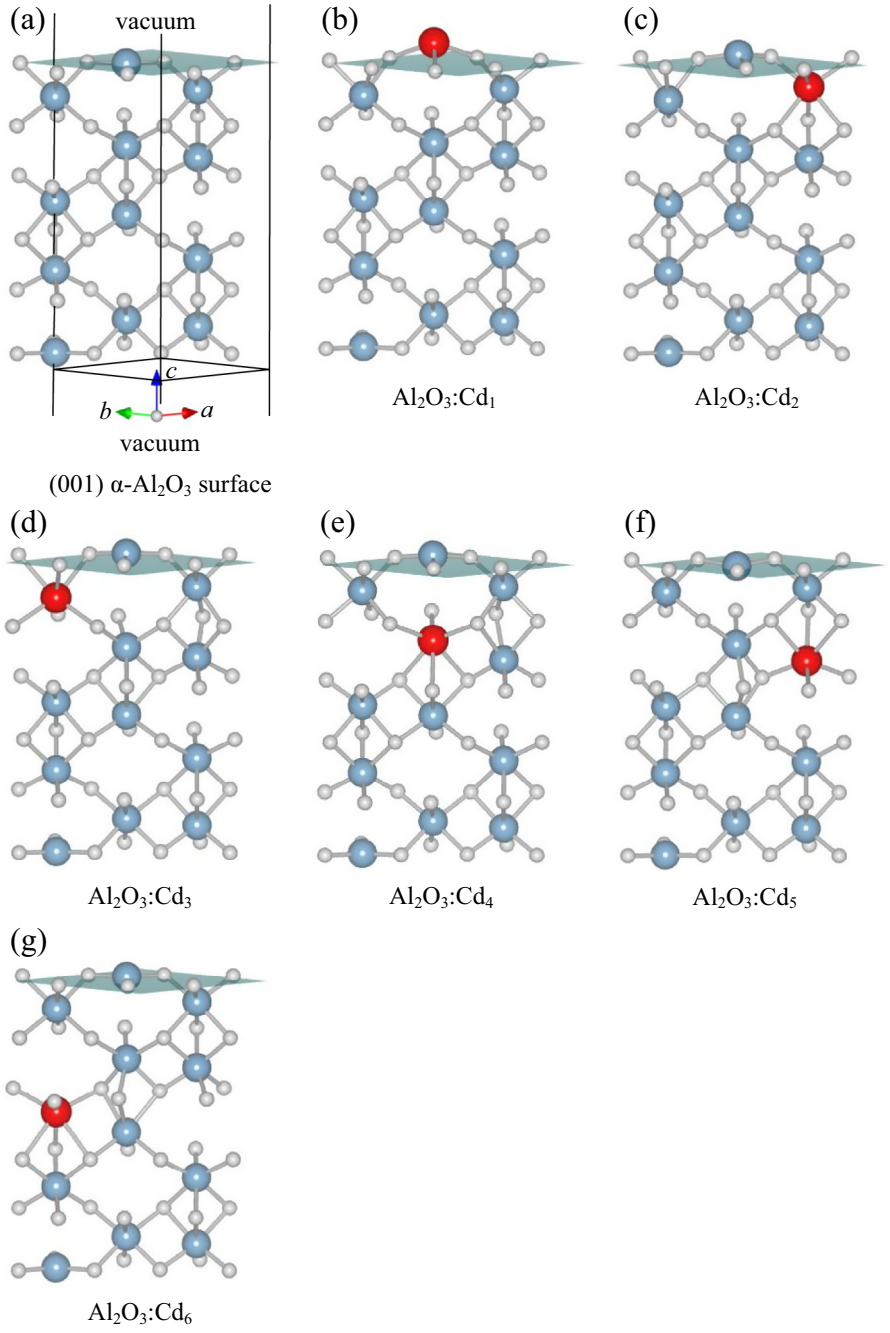

Fig. 1. Super-cells (equilibrium structures) used in the APW+lo calculations of (a) (0 0 1) pure α-Al_2O_3 surface and (b)–(g) Al_2O_3:Cd_1-Al_2O_3:Cd_6, respectively. In all cases the plane corresponding to $Z = 0$ Å (plane of the topmost Al atom in the (0 0 1) pure α-Al_2O_3 surface) is shown. The small (large) spheres represent O (Al) atoms. In (b)–(g) the Cd_i atom is identified as a red sphere. (For interpretation of the references to color in this figure legend, the reader is referred to the web version of this article.)

obtained from an equivalent plane-wave cutoff of 400 Ry. All the atomic positions were fully relaxed using a conjugate-gradient algorithm selecting a tolerance value for the forces of 0.02 eV/Å. The full Brillouin Zone was sampled with a Monkhorst Pack grid [37] of $10 \times 10 \times 1$. All these parameters ensure the convergence of both forces and total energy.

As mentioned before, SIESTA is a numerical and localized basis-set code, that allows performing faster geometrical optimizations when comparing with all-electron and planewaves-basis-set codes such as WIEN2k. This is true even in the case of no-symmetry, just considering the translational symmetry provided for the P1 crystallographic space group. However, since an important aim of this work is the determination of the EFG tensor, a pseudopotential-based program (such as SIESTA) is not able to account for this property. Hence, the EFG tensor is obtained using WIEN2k for the most stable structures obtained with SIESTA.

3. Results and discussion

In order to investigate whether the presence of Cd impurities localized at or below the surface produces a magnetic behavior, in opposition to the case of the pure surface or Cd-doped bulk Al_2O_3, we have calculated both the non spin-polarized and spin-polarized Cd-doped surface reconstruction. Both calculations predict basically the same relaxed final equilibrium atomic

positions but, as we will discuss below, the ground state for the doped surface is the spin-polarized solution.

In Fig. 1 we show the final equilibrium structure for all the cases studied here. Besides the expected Cd–ONN bond-length relaxation already observed in many Cd-doped binary oxides, the Cd atom is displaced along the [0 0 1] direction: while the Cd impurity in Al_2O_3:Cd_1 moves outwards from the surface, the rest move towards the surface, with the exception of the Al_2O_3:Cd_3 and Al_2O_3:Cd_5 systems in which the Cd atom is displaced towards the bulk. This apparently strange "up and down" behavior along the z axis of the Cd impurity relaxation (which is better appreciated in Fig. 2) is in fact correlated with the corundum crystalline structure, i.e., the Cd atoms moves always towards the O1 plane for each depth position (with exception of Cd_1, due to the broken of the crystal symmetry at the surface).

As expected, the reconstruction of the surface terrace as the Cd impurity moves away from the surface towards the bulk tends to that predicted for the pure α-Al_2O_3 [0 0 1] surface [22]. The final Cd–O1 and Cd–O2 bond-lengths and the displacement of the Cd impurity along the (0 0 1) axis are shown in Table 1 and Fig. 2. In this figure, the depth of the Cd atoms is referred to the position of the topmost Al atom in the pure optimized surface (Fig. 1a). The horizontal dashed lines are the positions of the native Al atom (replaced by the Cd atom) along the [0 0 1] axis in the pure surface. The largest displacement of Cd is obtained in the Al_2O_3:Cd_1 case, were the topmost Cd atom moves around 0.7 Å outwards from the surface. As can be observed in Fig. 2, the Cd–O1 and Cd–O2 bond-lengths tend to their values in Cd-doped bulk α-Al_2O_3, but for a depth of around 5 Å they are still slightly larger. It is worth mentioning that in the pure surface system the Al–O1 and Al–O2 bond-lengths are almost converged to the bulk values at this depth. As in the bulk case, the Cd–ONN bond-lengths after relaxation tend to the Cd–O distances corresponding to the most stable cadmium oxide, CdO ($d_{Cd-O_{CdO}}$ = 2.35 Å, solid (red)[1] vertical line in Fig. 2). It is noteworthy that, in the case of the doped surface, the Cd–O2 bond-length localized at about 3–5 Å from the surface is closer to the Cd–O_{CdO} bond-length than in the case of the doped bulk case. It is possible that in the Al_2O_3:Cd_5 and Al_2O_3:Cd_6 systems the ONN of the Cd impurity present lower structural constraints to relax (compared to those located into the bulk) due to the proximity of the surface.

In Fig. 3 we plot the total energy for all the systems studied at relaxed final equilibrium positions for spin-polarized calculations as a function of the depth of the Cd atoms from the surface, along the [0 0 1] direction. As we can see, the lowest energy corresponds to the Al_2O_3:Cd_1 case, i.e., when the Cd atom is located at the topmost substitutional Al site, which can be considered as a surface Cd deposition. In the rest of the cases the energy increases, and this behavior could be attributed to the induced stress in the Cd substitution that cannot be totally remove in the relaxation process. This effect could be partially compensated as we move inwards from the surface having the bulk-like relaxation behavior.

As mentioned before, the ground state of the Cd-doped surface is the spin-polarized solution when the Cd atom approaches to the surface, except for Al_2O_3:Cd_2 for which it is not possible to determine the ground state solution since the energy difference between magnetic and non-magnetic calculations is negligible. As we move into the bulk, both spin- and non spin- polarized calculations tend to the same total energy. In the case of the deepest Cd atom (Al_2O_3:Cd_6 system) both energies are the same, as occurs for Cd atoms located in bulk α-Al_2O_3 [18], and as suggested by the results coming from TDPAC experiments in ^{111}Cd-doped bulk

[1] For interpretation of color in Fig. 2, the reader is referred to the web version of this article.

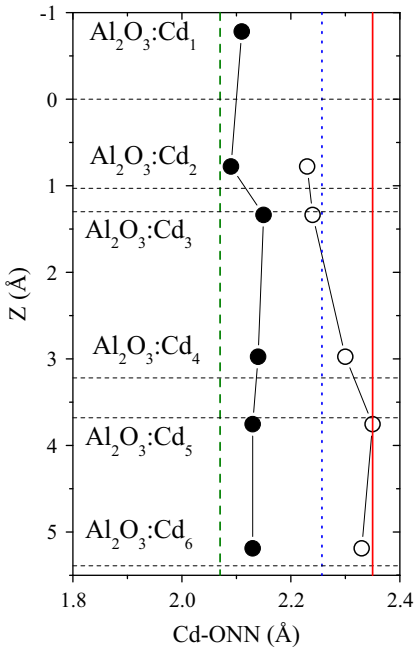

Fig. 2. Cd–O1 (black circles) and Cd–O2 (open circles) bond-lengths for the different depths of the Cd atom along the [0 0 1] direction from the surface, after relaxation. The Z = 0 Å is the position of the topmost Al atom in the (0 0 1) pure α-Al_2O_3 optimized surface. The vertical dashed and dotted lines are Cd–O1 and Cd–O2 bond-lengths in Cd–doped bulk Al_2O_3, respectively. The solid vertical line is the Cd–ONN bond-length in CdO. The horizontal dashed lines indicate the positions of the native Al atoms replaced by the Cd atoms in the reconstructed (0 0 1) pure α-Al_2O_3 surface.

Table 1
Cd–O1 and Cd–O2 bond-length and Cd displacement (in Å) for Al_2O_3:Cd_{1-6} systems and Cd-doped bulk α-Al_2O_3. The + (−) sign indicates that the Cd displacement (from the Al position in the reconstructed pure α-Al_2O_3 surface) is outward (inward) towards (from) the surface along the [0 0 1] direction.

	d Cd–O1	d Cd–O2	Cd displ.
Al_2O_3:Cd_1	2.11	–	+0.78
Al_2O_3:Cd_2	2.09	2.23	+0.25
Al_2O_3:Cd_3	2.15	2.24	−0.04
Al_2O_3:Cd_4	2.14	2.30	+0.24
Al_2O_3:Cd_5	2.13	2.35	−0.08
Al_2O_3:Cd_6	2.13	2.33	+0.20
Al_2O_3:Cd_{Bulk}	2.07	2.26	–

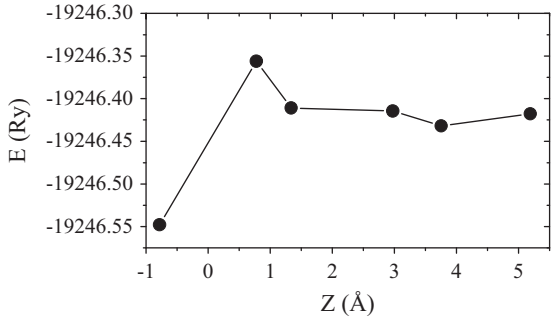

Fig. 3. Total energy for all the systems studied at relaxed final equilibrium positions as a function of the depth of the Cd atom from the surface, along the [0 0 1] direction. The Z = 0 Å is the position of the topmost Al atom in the (0 0 1) pure α-Al_2O_3 optimized surface.

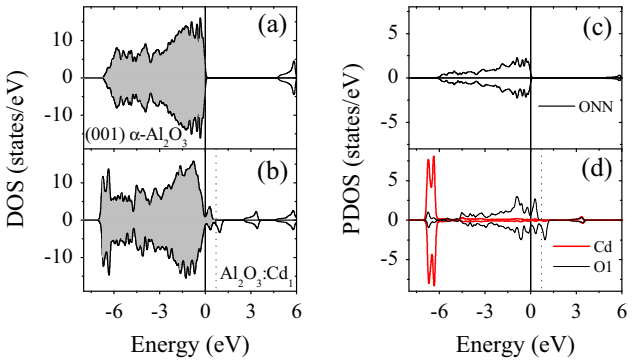

Fig. 4. Total density of states (DOS) for (a) pure α-Al_2O_3 and (b) Al_2O_3:Cd_1 (001) surfaces. Atom-resolved partial DOS for (c) pure α-Al_2O_3 and (d) Al_2O_3:Cd_1 (001) surfaces. The vertical lines indicate the top of the valence band (solid line) and the highest occupied state (dotted line). In (a) and (b) the grey region corresponds to occupied states.

α-Al_2O_3 [38,39], in which magnetic hyperfine interactions were not observed. It is interesting to note that the magnetic behavior that appears for Cd at the α-Al_2O_3 (001) surface is not present in pure surface. This could be understood in terms of the presence of localized states originated in under-coordinated nearest oxygen neighbors of the Cd atom localized near the surface, which are prone to be polarized in order to obtain a slight energetic stabilization of the system. In order to clarify this point we compare in Fig. 4 the density of states (DOS) and the atom-resolved partial density of states (PDOS) of the pure α-Al_2O_3 and Al_2O_3:Cd_1 (001) surfaces. The energy band gap in the pure surface is $\sim$1.5 eV smaller than the band gap in pure bulk α-Al_2O_3 (6.2 eV) [18], in agreement with the results of Ref. [5]. As we can see in Fig. 4(b and d), the presence of the Cd atom in the Al_2O_3:Cd_1 system introduces sharp electronic Cd states at the bottom of the valence band and induces and polarizes acceptor O1 states at the top of the valence band. For the rest of the systems (Al_2O_3:Cd_{2-6}), the polarization is produced over both O1 and O2 states, contributing each type of oxygen atom with different relative weights on the appearance of the magnetic moment (see Fig. 5, on the right). It is interesting to see the

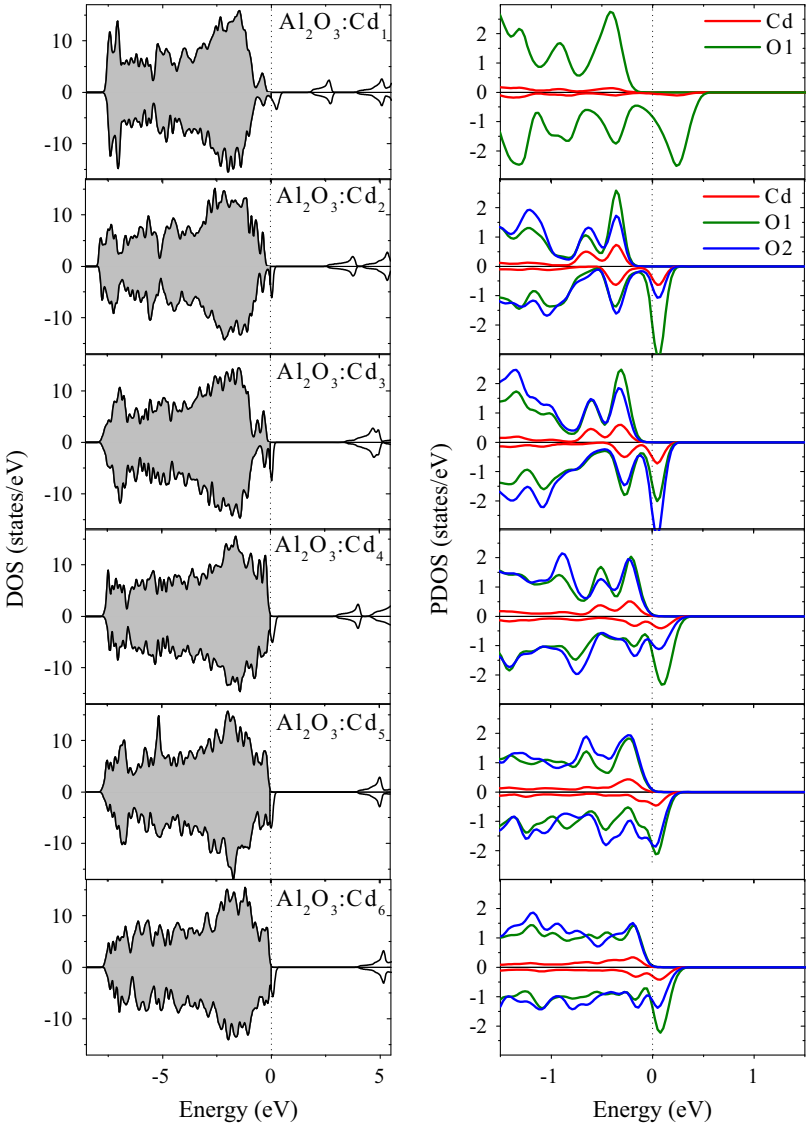

Fig. 5. Total density of states (DOS) (left) and partial density of states (PDOS) (right) projected at Cd and ONN atoms for Al_2O_3:Cd_{1-6} systems. The vertical dotted line indicates the highest occupied state.

behavior of the DOS as a function of the Cd depth from the surface. It is noteworthy to mention that DFT at the GGA level sub-estimates the value of the energy gap but, for comparison purposes, the methodology is valid and allow us to obtain trends along all the Cd substitutions [18]. The presence of the topmost Cd atom at the surface introduces empty O1 states in the middle of the band gap, reducing it to ~1.9 eV. This band gap is enlarged as long as the Cd atom moves from the surface into the bulk, obtaining for Al_2O_3:Cd_6 a band gap of 4.0 eV, around 20% smaller then the band gap of Cd-doped bulk α-Al_2O_3 [18]. This behavior is due to the displacement of O1 and O2 empty states, introduced by the presence of the Cd atom near the surface, towards the conduction band and the displacement of the acceptor impurity levels towards inside the top of the VB, as Cd moves into the bulk. The difference between the band gap energy of doped bulk α-Al_2O_3 and Al_2O_3:Cd_6 system is due to the difference already present between the band gap of the bulk and the surface in the pure system.

The behavior of the different contributions of Cd and ONN atoms to the total magnetic moment of the cell, which is 1.0 μ_B for all the doped systems studied here, is presented in Fig. 6. In Cd-doped bulk α-Al_2O_3 the total magnetic moment of the cell is also 1.0 μ_B, although the spin-polarized configuration is not the ground state [18]. The magnetic moment is in all cases mainly localized at the oxygen nearest neighbors to the Cd atom and in lesser extent (~10%) at the Cd site, with the exception of the topmost Cd atom case in which 90% of the magnetic moment of the cell is localized only at the three O1 atoms. As long as the Cd atom moves from the bulk to the surface, the magnetic moment becomes more localized at the O1 and O2 atoms. The sum of the rest of the contributions to the magnetic moment of the cell is around 10% at the surface and increases up to ~20% at 6 Å from the surface (difference between black squares and open circles in Fig. 6).

The predicted largest principal component V_{33} and the asymmetry parameter η of the EFG tensor are shown in Fig. 7. In it, over each V_{33} data point, an arrow indicates the V_{33} orientation with respect to the [001] crystal axis, being a vertical arrow parallel to this direction. As we can see for the topmost Cd atom, V_{33} is along the [001] direction, i.e., perpendicular to the surface. For the Al_2O_3:Cd_2 and Al_2O_3:Cd_3 systems, V_{33} is tilted with respect to the [001] direction and it recuperates the bulk [001] direction for deeper positions of the Cd atom.

When Cd moves away from the surface into the bulk ($Cd_2 \rightarrow Cd_{5-6}$), V_{33} tends to values slightly lower than bulk doped ones (dashed horizontal line). These relative lower values are in agreement with the slightly larger Cd–ONN bond-lengths in Al_2O_3:Cd_5 and Al_2O_3:Cd_6 in comparison to the bulk doped system. This is due to the r^{-3} dependence of the EFG, demonstrating the extremely sensitivity of this physical quantity to sense local structural distortions. Particularly, for the topmost Cd atom, the calculations predict axial symmetry ($\eta = 0$), as in bulk Cd-doped Al_2O_3. In Al_2O_3:Cd_1, it is important to mention that Cd presents only three nearest oxygen neighbors (O1) that relaxes in a symmetrical way, even though the structural optimization process in our procedure is not constrained by the symmetry imposed by the crystal structure (opposite to what occurs in other codes as, e.g., in Wien2k), enabling the prediction of η values different from zero. In some metal (e.g., Cu, In) and semiconductor (e.g., Si) free surfaces, V_{33} was experimentally determined applying the TDPAC method at (^{111}In→)^{111}Cd atoms *landed* on their surfaces, being its direction perpendicular to the surface (as in our predictions for the topmost Cd atom), fact that occurs even for different surfaces studied in the same compound [13–16,40]. In addition, and more impressive in the case of ^{111}Cd-doped metallic In thick film obtained by (^{111}In→)^{111}Cd evaporation/deposition in ultra high vacuum (UHV) conditions, the V_{33} value measured at ^{111}Cd atoms located at the surface is approximately 4 times larger than the value measured in bulk [13], in perfect agreement with our theoretical prediction, $V_{33}(Al_2O_3{:}Cd_1)/V_{33}(Al_2O_3{:}Cd\ bulk) = 3.8$ (see Fig. 7). In the case of the (1 1 0) Cu surface, the experimental V_{33} measured at ^{111}Cd atoms localized at substitutional terrace sites with respect to that determined at the subjacent 2nd and 3rd monolayers are about a factor of 1.6 and 8, respectively [16]. It should be noted that the bulk EFG in Cu vanishes due to its high lattice symmetry; hence a direct comparison of V_{33} values at surface and bulk sites is not possible.

Regarding the asymmetry parameter behavior near the surface, the abrupt increase in its value for Al_2O_3:Cd_2 and Al_2O_3:Cd_3 could be due to the fact that at these Cd atomic positions the ONN atoms (principal responsible for changes in the EFG at the Cd site) are bonded (in addition to the Cd atom) to Al atoms with very different character. For example, in Al_2O_3:Cd_2 (Al_2O_3:Cd_3) the O1 (O2) atoms are bonded with Al atoms located in the terrace of the surface,

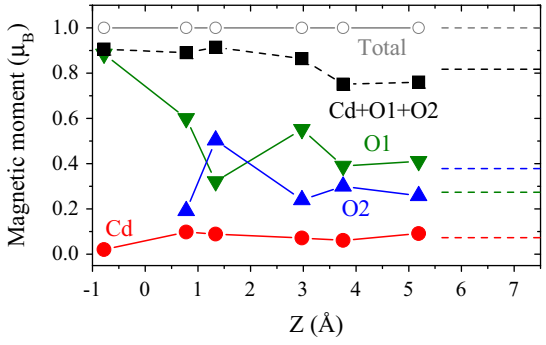

Fig. 6. Contributions of Cd, O1, and O2 atoms to the total magnetic moment of the cell as a function of the depth of the Cd atom from the surface, along the [001] direction. $Z = 0$ Å is the position of the topmost Al atom in the (001) pure α-Al_2O_3 optimized surface. The 3-fold multiplicity of O1 and O2 atoms has been considered. The horizontal dashed lines (on the right) show the partial contributions (in color) to the total (grey) magnetic moment of the cell for Cd-doped bulk α-Al_2O_3. (For interpretation of the references to color in this figure legend, the reader is referred to the web version of this article.)

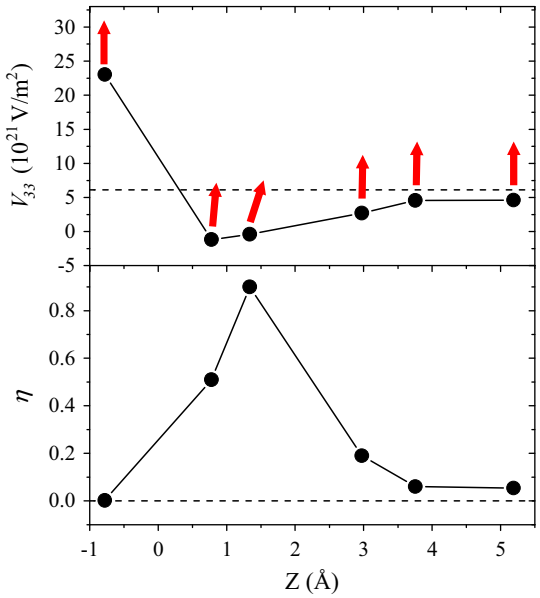

Fig. 7. Largest principal component V_{33} and asymmetry parameter η of the EFG tensor as a function of the depth of the Cd atom from the surface, along the [001] direction. $Z = 0$ Å is the position of the topmost Al atom in the pure α-Al_2O_3 (001) optimized surface. In both cases, the dashed horizontal line indicates the predicted values for bulk α-Al_2O_3.

whereas the O2 (O1) atoms are bonded with *bulk-like* Al atoms (Fig. 1). An increase of the η parameter at the different cation sites is absent in the reconstruction of the pure α-Al_2O_3 (001) surface, where the axial symmetry results to be preserved for all Al sites [22], even though the SIESTA code, which allows structural symmetry-breaking, was also applied to obtain the equilibrium positions of the atoms. The different behavior of the ONN displacements relative to the Cd site in the doped surface, which breaks the axial symmetry, must have its origin on the strong ONN relaxations produced by the presence of the impurity itself, fact that is absent during the atomic structural refinement of the pure surface reconstruction. All these strong differences in the EFG tensor found for different positions of the Cd atom above and below the Al_2O_3 surface could be valuable fingerprints of the ^{111}Cd probe localization in a real sample. For this reason, the combination of our results with key TDPAC experiments at surfaces, such as those of Refs. [13–16,40], could contribute to the understanding at the atomic level of growth, adsorption, and diffusion of atoms in oxide surfaces and interfaces, Al_2O_3 in particular.

Regarding the origin of the EFG, the contribution of Cd-*p* states to V_{33} dominates over the *d* contribution at the Cd_1 site. While at sites Cd_2 and Cd_3 the *p* and *d* contributions to V_{33} are of the same order of magnitude (and very much less intense), the *p* contribution dominates again over the *d* contribution for the deeper positions of the Cd atom, converging to the bulk behavior [18].

In Fig. 8(a) we plotted the electronic charge density corresponding to the impurity states localized at the top of the VB (with energies from −0.6 to 0 eV, see Fig. 5), $\rho^{imp}(\mathbf{r})$, for different representative depths of the Cd impurity from the surface. These $\rho^{imp}(\mathbf{r})$ were calculated at the (001) plane that contains each Cd_i atom, being those for Cd_{2-4} very similar between them and those for Cd_{5-6} very similar to the bulk. The more intense bonds point to the three O1 atoms in all cases, which are closer to the Cd atom and localized at a parallel plane.

Cd_1 makes bonds with the O1 atoms only; this fact could be the reason for having the most intense bond strength. These bonds present axial symmetry, in agreement with the null η parameter and with the V_{33} orientation normal to the (001) surface predicted

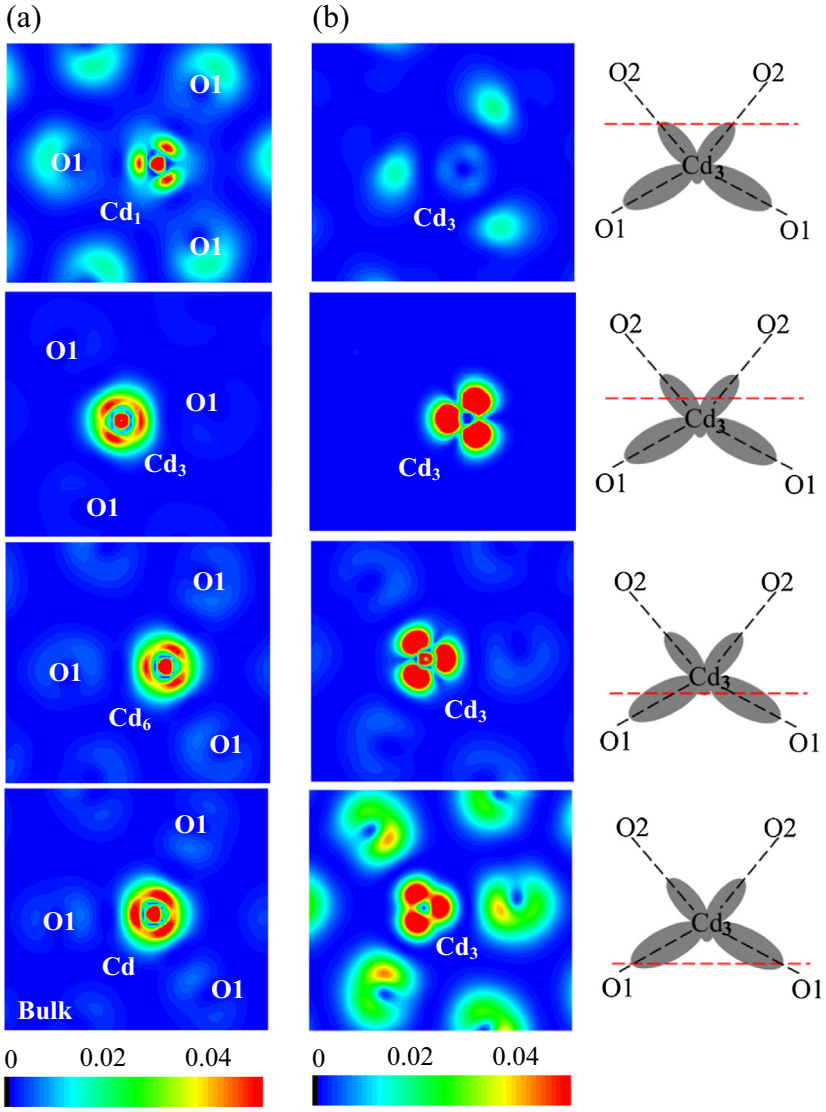

Fig. 8. Electronic charge density $\rho^{imp}(r)$ filtered at the impurity states localized at the top of the VB (see text) calculated at (a) planes parallel to the (001) plane, containing the Cd impurity at representative depths from the α-Al_2O_3 surface and in bulk, and (b) planes parallel to the (001) plane localized below and above the Cd_3 position. On the right, schematic drawing showing Cd3-O1 and Cd3-O2 bonds at a plane parallel to the [001] axis. The dashed (red) lines indicate the relative position along the [001] axis of the respective planes used in the calculation of each charge density plot of Fig. 8(b). (For interpretation of the references to color in this figure legend, the reader is referred to the web version of this article.)

at the terrace position. One way to roughly evaluate apparent changes in the EFG tensor is to inspect the relative weights of the different filled orbital components (p_i and d_i) of the relevant contributions (p and d) to the EFG. These *partial charges* are obtained integrating the different Cd-projected PDOS along the complete energy range of the valence band (see Ref. [18] for a detailed description of *partial charges* calculation). The anomalous extremely high V_{33} value found at this site has to be correlated with a high asymmetry in the partial charges p_x, p_y, and p_z of these bonds, since the p-contribution to the EFG is dominant at this Cd position. In effect, a close inspection to the Cd-projected PDOS of p-states along the VB shows that p_x and p_y are almost equal and very different with respect to p_z (see Fig. 9), giving a high V_{33} modulus.

The other 3 oxygen atoms near Cd_1 are second nearest oxygen neighbors (ONNN), which are coplanar to the precedent O1 atoms and a little amount of charge points towards them. These ONNN atoms are also seen at Cd_3, Cd_6, and for the bulk, but with a much less intensity (Fig. 8a).

At Cd_2 and Cd_3 the asymmetry parameter η is very high and V_{33} is almost null, even smaller than the bulk value. At these sites the Cd-projected p-states along the VB are much more equal between them than in the case of Cd_1 (see Fig. 9), in agreement with the strong decrease of the p-contribution. Also, the p-contribution has the same order of magnitude than the d one, contributing to diminish the total EFG at these sites. In these cases, in which the d-contribution to the EFG is relevant, it is interesting to inspect with more detail $\rho^{\mathrm{imp}}(\mathbf{r})$ at, e.g., Cd_3 (see Fig. 8a, 2nd row), since in general the impurity levels localized at the top of the VB have essentially d-character. In this plot the asymmetry in intensity of the Cd_3-O1 bonds is observed, in agreement with the high η parameter predicted (this parameter reflects the asymmetry in the coordination geometry) and the tilted orientation of V_{33} with respect to the [001] crystal axis. In addition, this asymmetry should modify the relative weights of the partial charges of d-symmetry (and also those of p-character), affecting the total EFG, as shown by the V_{33} calculation. In this plot (in green) it is also apparent the presence of other bonds, 60° shifted from the Cd–O1 ones. These bonds could be the images at this plane of the Cd coordination with the ONNN atoms (coplanar with the O1 atoms) or with the coordination with the O2 atoms that are in another parallel plane. To resolve this, in Fig. 8(b) we have plotted $\rho^{\mathrm{imp}}(\mathbf{r})$ at different planes parallel to the (001) surface, and very close to the Cd_3 atom. When we move towards the O1 atoms, the Cd–O1 bonds are enlightened, without the green contribution that was shifted 60° from this one. If we move towards the O2 atoms, the Cd–O2 bonds are now only present, showing that the green charge contribution at Cd_3 in Fig. 8(a) was the image of the Cd–O2 bonds and not that of the Cd–ONNN ones. This charge is less intense just because of the smaller Cd–O2 bond-strength and it disappears in the first plot (Fig. 8(b), 1st row) because the Cd–O2 bond is concentrated nearer the Cd atom than in the Cd–O1 bond.

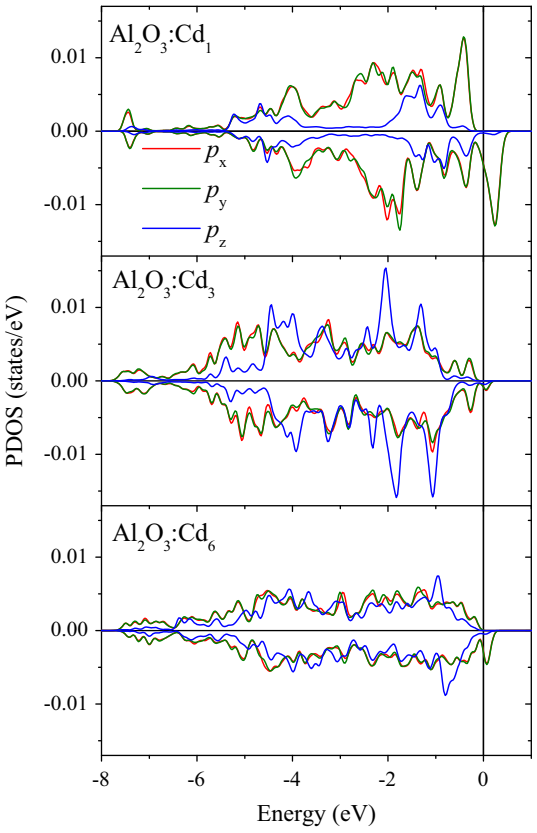

Fig. 9. Cd-projected PDOS p_x, p_y, and p_z for α-Al_2O_3:Cd_1, α-Al_2O_3:Cd_3, and α-Al_2O_3:Cd_6 systems.

Finally, the inspection of $\rho^{\mathrm{imp}}(\mathbf{r})$ at Cd_6 is very similar to that for Cd in bulk, with Cd–O1 bonds more intense than the Cd–O2 ones (see Fig. 8(a)). At this site $\rho^{\mathrm{imp}}(\mathbf{r})$ is again axially symmetric, in agreement with the prediction of a null η parameter and a V_{33} orientation parallel to the [001] axis, as in bulk. The magnitude of V_{33}, as mentioned before, is 4 times lower than that at the Cd_1 site. This can be understood knowing that the p-contribution to V_{33} is again dominant, as for Cd_1, but at Cd_6 and at the bulk case now the charge density is shared in two different groups of symmetric bonds, Cd–O1 and Cd–O2, distributing the electronic charge more homogenously in space, reducing the difference among the p-partial charges, lowering the magnitude of V_{33}. In effect, if we inspect the p-PDOS corresponding to Cd_6 (see Fig. 9), it is evident that they are all very similar, explaining why the V_{33} magnitude in Cd_6 is lower than in Cd_1.

When evaluating the relative stability of a Cd atom doping this oxide at different depths from the surface, it is observed that the most stable configuration corresponds to the superficial doping (Al_2O_3:Cd_1), as Fig. 3 shows. In this case, most of the strain is concentrated at Cd and its ONN atoms. This is not the case for the rest of the systems, in which the strain is transferred also to next nearest Al and O atoms. Subsurface doping, i.e. $Z > 0$ Å, is unfavorable when compared to surface doping, nevertheless the total energy decreases as we go deeper into the structure. This result could indicate that superficial Cd atoms will hardly diffuse into the Al_2O_3 material, but once this energy barrier is jumped (e.g. using ion implantation), they could diffuse into the bulk under certain external physical conditions such as thermal treatments. Considering the similar electronic configurations of Cd and In, this scenario is in agreement with the difficulty observed to diffuse ^{111}In(→^{111}Cd) atoms into Al_2O_3 bulk samples using only thermal treatments in order to localize ^{111}Cd atoms at substitutional Al sites [41], in opposition to the efficiency of ion implantation doping in PAC experiments [38,39]. On the other hand, a Cd atom located deep enough into the surface (around 5 Å), will hardly diffuse to the external surface of the Al_2O_3 slab, even though it can diffuse rather easily from the bulk towards the surface [41]. It is important to mention that these statements are just based in relative energies, and that kinetic aspects have not been considered.

4. Conclusions

Applying a double theoretical approach for the surface reconstruction and the electronic structure calculation of the (001) α-Al_2O_3 surface using SIESTA and the APW+lo method,

respectively, we have investigated the structural, electronic, magnetic, and hyperfine consequences of Cd doping for different depths of the impurity from the surface.

For the most stable (001) α-Al_2O_3 surface, we demonstrated that the inclusion of the Cd atom at substitutional Al sites produces a ground state magnetic behavior at and near the surface. As long as the Cd atom goes deeper into the bulk, the energy difference between polarized and non polarized solutions vanishes as occurs in the bulk. The total magnetic moment for all depths is 1.0 μ_B, and is mainly localized at the O1 atoms for the topmost Cd_1 atom, and at O1 and O2 for the rest of the $Cd_{2\text{-}6}$ positions.

The EFG at Cd_1 atom localized just above the α-Al_2O_3 terrace showed the same [001] orientation and a dominating *p*-contribution to V_{33} as at Cd substitutional sites in bulk Al_2O_3, but exhibits an anomalous V_{33} magnitude four times larger than the value in bulk. This change in V_{33} has been explained in terms of the very different behavior of the Cd-*p* states for both extreme situations.

The structural asymmetric relaxation around the Cd impurity produced just below the surface (Cd_2–Cd_3) is responsible for the strong change in the asymmetry (high η parameter), magnitude, and orientation of the EFG tensor. The almost null value of V_{33} at these Cd positions is due to the strong decrease of the *p*-contribution to V_{33} that results in the same order of magnitude but with opposite sign than the *d*-contribution. All these changes in the hyperfine properties have been correlated with the modifications observed on the electronic charge density at the different Cd depths from the surface and on the PDOS of the Cd *p*-states.

The significant differences on the hyperfine parameters showed for different depths demonstrate that the ^{111}Cd probes could be used as efficient TDPAC probes for evaluating geometrical and electronic distortions, particularly for positions quite close to the reconstructed surface. Important electronic structure properties have been obtained and explained in terms of the local geometrical distortions, thus explaining the origin of the observed changes in the EFG. We hope that the highly local sensitivity demonstrated for ^{111}Cd probe-atoms to structural and electronic changes in their subnanoscopic neighborhood at and near the Al_2O_3 surface could also contribute to studies of growth, adsorption, and diffusion of atoms in oxide surfaces and interfaces through the development of dedicated TDPAC experiments in these kind of systems.

All these results suggest that the systems could present interesting potentialities facing new technological challenges like Quantum Computation. In particular, the capability to passivate the magnetic noise in qubits systems based on (001) α-Al_2O_3 surfaces doped with Cd atoms at different depths should be investigated in the future from first-principles.

Acknowledgment

This work was partially supported by Consejo Nacional de Investigaciones Científicas y Técnicas (CONICET) under grant N° PIP0002, Argentina. This research made use of the HP-Parallel-Computing Bose Cluster, and the computational facilities of the Physics of Impurities in Condensed Matter group, at Instituto de Física La Plata and Departamento de Física. RF wishes to thank the Uruguayan funding institutions: CSIC, ANII and PEDECIBA.

Appendix A. Supplementary material

Supplementary data associated with this article can be found, in the online version, at http://dx.doi.org/10.1016/j.commatsci.2015.04.008.

References

[1] T.S. Santos, J.S. Lee, P. Migdal, I.C. Lekshmi, B. Satpati, J.S. Moodera, Phys. Rev. Lett. 98 (2007) 16601.
[2] V. Dediu, L.E. Hueso, I. Bergenti, A. Riminucci, F. Borgatti, P. Graziosi, C. Newby, F. Casoli, M.P. De Jong, C. Taliani, Y. Zhan, Phys. Rev. B 78 (2008) 115203.
[3] G. Kresse, M. Schmid, E. Napetschnig, M. Shishkin, L. Kohler, P. Varga, Science 308 (2005) 1440–1442.
[4] H. Li, J. Feng, W. Zhang, W. Jiang, H. Gu, J.R. Smith, Phys. Rev. B 80 (2009) 205422.
[5] D. Lee, J.L. DuBois, V. Lordi, Phys. Rev. Lett. 112 (2014) 017001.
[6] G. Schatz, A. Weidinger, Nuclear Condensed Matter Physics: Nuclear Methods and Applications, Wiley, Chichester, England, 1996.
[7] N.E. Kaufmann, R.J. Vianden, Rev. Mod. Phys. 51 (1979) 161–214.
[8] S. Zhu, G. Zhang, F. Li, D. Yuan, in: Proceedings of the 4th Joint International Conference on Hyperfine Interactions and International Symposium on Nuclear Quadrupole Interactions, Springer, Dordrecht, Netherlands, 2013.
[9] L.A. Errico, G. Fabricius, M. Rentería, Phys. Rev. B 67 (2003) 144104.
[10] G.N. Darriba, L.A. Errico, P.D. Eversheim, G. Fabricius, M. Rentería, Phys. Rev. B 79 (2009) 115213.
[11] M. Forker, P. de la Presa, W. Hoffbauer, S. Schalabach, M. Bruns, D.B. Szabó, Phys. Rev. B 77 (2008) 54108.
[12] H. Jaeger, M.O. Zacate, Defect and Diffusion Studied Using PAC Spectroscopy, Trans Tech Publications Ltd., Zurich, Switzerland, 2011.
[13] W. Körner, W. Keppner, B. Lehndorff-Junges, G. Schatz, Phys. Rev. Lett. 49 (1982) 1735–1738.
[14] T. Klas, J. Voigt, W. Keppner, R. Wesche, G. Schatz, Phys. Rev. Lett. 57 (1986) 1068–1071.
[15] T. Klas, R. Fink, G. Krausch, R. Platzer, J. Voigt, R. Wesche, G. Schatz, Europhys. Lett. 7 (1988) 151–157.
[16] T. Klas, R. Fink, G. Krausch, R. Platzer, J. Voigt, R. Wesche, G. Schatz, Surface Sci. 216 (1989) 270–302.
[17] L.A. Errico, G. Fabricius, M. Rentería, P. de la Presa, M. Forker, Phys. Rev. Lett. 89 (2002) 055503.
[18] G.N. Darriba, M. Rentería, H.M. Petrilli, L.V.C. Assali, Phys. Rev. B 86 (2012) 075203.
[19] G.N. Darriba, E.L. Muñoz, L.A. Errico, M. Rentería, J. Phys. Chem. C 118 (2014) 19929–19939.
[20] P. Hohenberg, W. Kohn, Phys. Rev. 136 (1964) B864–B871.
[21] W. Kohn, L.J. Sham, Phys. Rev. 140 (1965) A1133–A1138.
[22] G.N. Darriba, R. Faccio, M. Rentería, Phys. B 407 (2012) 3093–3095.
[23] F. Izumi, H. Asano, H. Murata, N. Watanabe, J. Appl. Cryst. 20 (1987) 411–418.
[24] P. Guénard, G. Renaud, A. Barbier, M. Gautier-Soyer, Surf. Rev. Lett. 5 (1998) 321–324.
[25] J. Ahn, J.W. Rabalais, Surf. Sci. 388 (1997) 121–131.
[26] T. Suzuki, S. Hishita, K. Oyoshi, R. Souda, Surf. Sci. 437 (1999) 289–298.
[27] P. Blaha, K. Schwarz, G. Madsen, D. Kvasnicka, J. Luitz, WIEN2k, An Augmented Plane Wave Plus Local Orbitals Program for Calculating Crystal Properties; Technical Universität Wien, Austria, 1999.
[28] E. Sjöstedt, L. Nordström, D.J. Singh, Solid State Commun. 114 (2000) 15–20.
[29] G.K.H. Madsen, P. Blaha, K. Schwarz, E. Sjöstedt, L. Nordström, Phys. Rev. B 64 (2001) 195134.
[30] K. Schwarz, C. Ambrosch-Draxl, P. Blaha, Phys. Rev. B 42 (1990) 2051–2061.
[31] J.P. Perdew, Y. Wang, Phys. Rev. B 45 (1992) 13244–13249.
[32] J.P. Perdew, K. Burke, M. Ernzerhof, Phys. Rev. Lett. 77 (1996) 3865–3868.
[33] P. Ordejón, E. Artacho, J.M. Soler, Phys. Rev. B 53 (1996) R10441–R10444.
[34] D. Sánchez-Portal, P. Ordejón, E. Artacho, J.M. Soler, Int. J. Quantum Chem. 65 (1997) 453–461.
[35] J.M. Soler, E. Artacho, J.D. Gale, A. García, J. Junquera, P. Ordejón, D. Sánchez-Portal, J. Phys.: Condens. Matter 14 (2002) 2745–2779.
[36] N. Troullier, J.L. Martins, Phys. Rev. B 43 (1991) 1993–2006.
[37] H.J. Monkhorst, J.D. Pack, Phys. Rev. B 13 (1976) 5188–5192.
[38] S. Habenicht, D. Lupascu, M. Neubauer, M. Uhrmacher, K.P. Lieb, Hyp. Int. 120/121 (1999) 445–448.
[39] J. Penner, R. Vianden, Hyp. Int. 158 (2005) 389–394.
[40] G. Kraush, T. Detzel, R. Fink, B. Luckscheiter, R. Platzer, U. Wöhrmann, G. Shatz, Phys. Rev. Lett. 68 (1992) 377–380.
[41] M. Rentería, Personal Communication.